Upregulation of reduced folate carrier by vitamin D enhances brain folate uptake in mice lacking folate receptor alpha

Camille Alam[a], Susanne Aufreiter[b], Constantine J. Georgiou[a], Md. Tozammel Hoque[a], Richard H. Finnell[c,d], Deborah L. O'Connor[b,e], I. David Goldman[f,g], and Reina Bendayan[a,1]

[a]Department of Pharmaceutical Sciences, Leslie Dan Faculty of Pharmacy, University of Toronto, Toronto, ON M5S 3M2, Canada; [b]Translational Medicine Program, The Hospital for Sick Children, Toronto, ON M5G 0A4, Canada; [c]Department of Molecular and Cellular Biology, Baylor College of Medicine, Houston, TX 77030; [d]Department of Medicine, Baylor College of Medicine, Houston, TX 77030; [e]Department of Nutritional Sciences, University of Toronto, Toronto, ON M5S 1A8, Canada; [f]Department of Medicine, Albert Einstein College of Medicine, Bronx, NY 10461; and [g]Department of Molecular Pharmacology, Albert Einstein College of Medicine, Bronx, NY 10461

Edited by Patrick J. Stover, Texas A&M AgriLife Research, Ithaca, NY, and approved July 11, 2019 (received for review April 25, 2019)

Folates are critical for central nervous system function. Folate transport is mediated by 3 major pathways, reduced folate carrier (RFC), proton-coupled folate transporter (PCFT), and folate receptor alpha (FRα/Folr1), known to be regulated by ligand-activated nuclear receptors. Cerebral folate delivery primarily occurs at the choroid plexus through FRα and PCFT; inactivation of these transport systems can result in very low folate levels in the cerebrospinal fluid causing childhood neurodegenerative disorders. These disorders have devastating effects in young children, and current therapeutic approaches are not sufficiently effective. Our group has previously reported in vitro that functional expression of RFC at the blood–brain barrier (BBB) and its upregulation by the vitamin D nuclear receptor (VDR) could provide an alternative route for brain folate uptake. In this study, we further demonstrated in vivo, using Folr1 knockout (KO) mice, that loss of FRα led to a substantial decrease of folate delivery to the brain and that pretreatment of Folr1 KO mice with the VDR activating ligand, calcitriol (1,25-dihydroxyvitamin D_3), resulted in over a 6-fold increase in [$^{13}C_5$]-5-formyltetrahydrofolate ([$^{13}C_5$]-5-formylTHF) concentration in brain tissues, with levels comparable to wild-type animals. Brain-to-plasma concentration ratio of [$^{13}C_5$]-5-formylTHF was also significantly higher in calcitriol-treated Folr1 KO mice (15-fold), indicating a remarkable enhancement in brain folate delivery. These findings demonstrate that augmenting RFC functional expression at the BBB could effectively compensate for the loss of Folr1-mediated folate uptake at the choroid plexus, providing a therapeutic approach for neurometabolic disorders caused by defective brain folate transport.

brain folate transport | blood–brain barrier | vitamin D receptor

Folates are required for key biosynthetic processes in mammalian cells (1). Mammals must obtain folates from their diet since they lack the enzymatic capacity for folate biosynthesis; maintaining sufficient levels of folates requires effective gastrointestinal absorption and tissue distribution. Folate transport is mediated by 3 major pathways: folate receptor alpha (FRα; *FOLR1*), proton-coupled folate transporter (PCFT; *SLC46A1*), and reduced folate carrier (RFC; *SLC19A1*). FRα is a cell surface glycoprotein that binds folate with high affinity (Michaelis constant [K_m] = 1 to 10 nM) and facilitates transport through receptor-mediated endocytosis (2, 3). PCFT, which exhibits a lower affinity for folates (K_m = 1 μM) compared with FRα, is a proton cotransporter with optimal activity at pH 5.5, and is responsible for the majority of intestinal folate absorption (4, 5). RFC has a comparable affinity as PCFT (K_m = 2 to 7 μM) for reduced folate uptake at physiological pH, and is an antiporter that exchanges folates with intracellular organic phosphates (6).

Folates are critical for the development and function of the central nervous system (CNS). Brain folate transport is primarily mediated by concerted actions of FRα and PCFT at the choroid plexus. Folate uptake is initiated by FRα-mediated transcytosis across the choroid plexus epithelium, followed by the export of folates from FRα-containing exosomes directly into the cerebrospinal fluid (CSF) presumably via PCFT (7, 8). PCFT-mediated folate export from acidified endosomes may also occur within the cytoplasm of epithelial cells in order to maintain the function of the choroid plexus (7). Inactivation of FRα causing cerebral folate deficiency (9, 10) or inactivation of PCFT causing hereditary folate malabsorption (4, 8) through loss-of-function mutations or the presence of FRα autoantibodies (11) can severely impair brain folate uptake, thereby resulting in very low CSF folate levels and causing early childhood neurodegenerative disorders. While rare, these disorders have devastating effects in young children. Hereditary folate malabsorption presents within a few months after parturition, and is characterized by anemia and failure to thrive, followed by developmental delays, abnormal brain myelination, psychomotor regression, ataxia, and recurrent seizures (4, 8). Loss of FRα shares similar neurological defects as with loss of PCFT, but signs of this disorder only present several years after birth. This delay in onset may be due to normal intestinal absorption and blood folate levels that continuously provide folates to the developing brain, albeit at reduced levels (9, 10).

Significance

Folates are critical for brain development and function. Abnormalities in brain folate transport have been implicated in a number of childhood neurodevelopmental disorders, including cerebral folate deficiency syndrome, hereditary folate malabsorption, and autism spectrum disorders. These disorders have devastating effects in young children, and current therapeutic approaches are not sufficiently effective. In this study, we demonstrate that functional expression of the folate transporter, reduced folate carrier, at the blood–brain barrier and its upregulation by the vitamin D nuclear receptor can remarkably increase folate transport to the brain. These findings provide a strategy for enhancing brain folate delivery for the treatment of neurometabolic disorders caused by folate transport defects.

Author contributions: C.A., S.A., D.L.O., and R.B. designed research; C.A., S.A., C.J.G., and M.T.H. performed research; R.H.F., D.L.O., and R.B. contributed new reagents/analytic tools; C.A., S.A., C.J.G., and R.B. analyzed data; and C.A., I.D.G., and R.B. wrote the paper.

The authors declare no conflict of interest.

This article is a PNAS Direct Submission.

Published under the PNAS license.

[1]To whom correspondence may be addressed. Email: r.bendayan@utoronto.ca.

This article contains supporting information online at www.pnas.org/lookup/suppl/doi:10.1073/pnas.1907077116/-/DCSupplemental.

Published online August 12, 2019.

The 3 major folate transport pathways are modulated, in part, by nuclear receptors. These receptors are DNA-binding transcription factors that regulate the functional expression of target genes in the presence of specific ligand activators (12). The vitamin D receptor (VDR), in particular, has been reported to regulate PCFT functional expression in the intestine. Eloranta et al. (13) demonstrated that treatment of intestinal Caco-2 cells and isolated rat duodenum with the VDR-activating ligand, 1,25-dihydroxyvitamin D_3 [$1,25(OH)_2D_3$ or calcitriol] induced *SLC46A1*/*Slc46a1* (PCFT) messenger RNA (mRNA) expression, which subsequently increased folic acid uptake. Recently, our laboratory has also examined the role of VDR in the regulation of RFC at the blood–brain barrier (BBB) (14). We provided evidence that activation of VDR through calcitriol exposure upregulates RFC mRNA and protein expression, as well as function, in immortalized cultures of human brain microvessel endothelial cells (hCMEC/D3) and isolated mouse brain capillaries that are representative of the BBB. Our study also showed that RFC expression was down-regulated by VDR-targeting small interfering RNA, further suggesting a role for VDR in the regulation of this folate transporter.

To date, brain folate transport has been primarily characterized at the choroid plexus. However, in cases where FRα or PCFT function is compromised, functional expression of RFC at the BBB may constitute an alternative pathway for folate delivery into the CNS. Furthermore, induction of RFC via interactions with specific nuclear receptors, such as VDR, may enhance transport of folate into the brain. Several groups, including ours, have confirmed the presence of RFC in human (14, 15) and rodent (16) BBB, and demonstrated active transport of folates in various BBB model systems, including isolated human brain capillaries (17), immortalized human cell lines (hCMEC/D3), and rat (RBE4) cerebral microvessel endothelium (14, 15). The objective of the current study was to investigate the role of VDR in the regulation of RFC in vivo, using a FRα/Folr1 knockout (KO) mouse model. Modulating folate uptake at the BBB through RFC could potentially represent a novel strategy for the treatment of neurometabolic disorders resulting from failure of folate transport across the choroid plexus.

Materials and Methods

Materials. All cell culture reagents were obtained from Invitrogen, unless indicated otherwise. Real-time qPCR reagents, such as reverse transcription complementary DNA (cDNA) kits and qPCR primers, were purchased from Applied Biosystems and Life Technologies, respectively. Primary rabbit polyclonal AE390 anti-RFC antibody was kindly provided by one of the authors (I.D.G.). Primary rabbit polyclonal anti-HCP1 (ab25134) and anti-FBP (ab67422) antibodies were obtained from Abcam. Mouse monoclonal anti-Na^+/K^+-adenosinetriphosphatase α (ATPase α; sc-58628) antibody was purchased from Santa Cruz Biotechnology. Anti-rabbit Alexa Fluor 594– and anti-mouse Alexa Fluor 488–conjugated secondary antibodies were supplied by Invitrogen. Calcitriol [$1,25(OH)_2D_3$] was obtained from Cayman Chemical Company. Isotopically labeled (glutamyl-$^{13}C_5$) 5-formyltetrahydrofolate ([$^{13}C_5$]-5-formylTHF), 5-methyltetrahydrofolate ([$^{13}C_5$]-5-methylTHF), folic acid ([$^{13}C_5$]-folic acid), and corresponding unlabeled folates were synthesized by Merck Eprova AG and generously provided to us by one of the authors (D.L.O.). All liquid chromatography-tandem mass spectrometry (LC-MS/MS) reagents and standard laboratory chemicals were purchased from Sigma–Aldrich.

Cell Culture. Primary cultures of mouse brain microvascular endothelial cells (C57BL/6 strain) were kindly provided by I. Aubert, Sunnybrook Health Sciences Centre, Toronto, ON, Canada. Cells (passages 2 to 4) were cultured in mouse endothelial cell basal medium supplemented with vascular endothelial growth factor, endothelial cell growth supplement, heparin, epidermal growth factor, hydrocortisone, L-glutamine, fetal bovine serum, and antibiotic-antimycotic solution (Cell Biologics). Cells were grown in flasks coated with gelatin-based solution, maintained in a humidified incubator at 37 °C (5% CO_2, 95% air atmosphere), and subcultured with 0.25% trypsin-ethylenediaminetetraacetic acid (EDTA) upon reaching 80% confluence. Culture medium was replaced every 2 to 3 d.

Mouse Brain Capillary Isolation. Brain capillaries were isolated from adult male or female LM/Bc mice (8 to 12 wk old) as described previously (14, 18). Mice were anesthetized through isoflurane inhalation and decapitated once a deep anesthetic surgical plane was achieved. Brains were immediately removed, and cortical gray matter was homogenized in ice-cold isolation buffer (i.e., phosphate-buffered saline [PBS] containing calcium and magnesium and supplemented with 5 mM glucose and 1 mM sodium pyruvate). Ficoll solution (30% final concentration) was added to the brain homogenates, and the mixture was centrifuged at 5,800 × *g* for 20 min at 4 °C. The resulting pellet of capillaries was resuspended in ice-cold isolation buffer supplemented with 1% bovine serum albumin (BSA) and filtered through a 300-μm nylon mesh. The filtrate was passed through a 30-μm pluriStrainer and washed with 50 mL of isolation buffer containing 1% BSA. Capillaries were harvested with 50 mL of isolation buffer and centrifuged at 1,600 × *g* for 5 min. The resulting pellet containing the capillaries was snap-frozen in liquid nitrogen until further analysis.

Immunocytochemical Analysis. Subcellular localization of RFC, PCFT, and FRα proteins was investigated by laser confocal microscopy in primary cultures of mouse brain microvascular endothelial cells representative of the BBB. Cells were grown as a monolayer on gelatin-coated glass coverslips and fixed with 4% paraformaldehyde for 20 min at room temperature (RT). Cells were then washed 4 times with PBS and permeabilized with 0.1% Triton X-100 for 5 min at RT as described previously (19). Nonspecific sites were blocked with 0.1% (mass/volume [m/v]) BSA and 0.1% (m/v) skim milk solution for 1 h before incubation with primary antibodies for 1.5 h at 37 °C, followed by overnight incubation at 4 °C in a humidified condition. Primary rabbit polyclonal AE390 anti-RFC (1:50), anti-HCP1 (1:50), and anti-FBP (1:50) were used to detect RFC, PCFT, and FRα proteins, respectively. Mouse monoclonal anti-Na^+/K^+-ATPase α (1:50) was used to visualize the plasma membrane. Following primary antibody incubation, cells were washed with PBS 4 times by gentle agitation and incubated with anti-rabbit Alexa Fluor 594– or anti-mouse Alexa Fluor 488–conjugated secondary antibodies (1:500) for 1.5 h at 37 °C. Cell staining without primary antibodies was used as a negative control. Following secondary antibody incubation, cells were washed again 4 times with PBS and mounted on a 76 × 26 microscope slide (VWR) using SlowFade Gold Antifade Mountant with DAPI (S36938; Invitrogen). Cells were visualized using an LSM 700 laser-scanning confocal microscope (Carl Zeiss AG) operated with ZEN software. Three-dimensional colocalization of folate transporters/receptor to the plasma membrane marker, Na^+/K^+-ATPase α, was quantified using Imaris Bitplane software (Oxford Instruments).

Animal Model. Folr1 KO and wild-type (WT) mice of the LM/Bc background strain were developed and kindly provided by one of the authors (R.H.F.) (20). Functional inactivation of *Folr1* produces mouse embryos with severe growth retardation and developmental abnormalities causing in utero death by gestational day 10 (21). To prevent embryonic lethality, heterozygous females were supplemented with 40 mg/kg of dietary folic acid starting from 2 wk before mating and continued throughout the gestational period (Research Diets). Following birth, this supplementation was no longer required and mice were maintained on an AIN-93G casein-based semipurified diet designed to meet all nutritional requirements for the growing mouse, including 2 mg/kg of folic acid and 0.0375 mg/kg of vitamin D. Genotypes of adult mice (2 to 3 wk of age) were determined by PCR analysis of genomic DNA extracted from ear punch samples as described previously (20). All mice were housed in clear polycarbonate microisolator cages, allowed free access to food and water, and maintained on a 14:10 light/dark cycle. All experiments, procedures, and animal care were conducted in accordance with the Canadian Council on Animal Care guidelines and approved by the University of Toronto Animal Care Committee.

Calcitriol [$1,25(OH)_2D_3$] Treatment in Mice. Calcitriol in powdered form was initially dissolved in anhydrous ethanol, and the concentration was measured spectrophotometrically at 265 nm (UV-1700; Schimadzu Scientific Instruments) before diluting in sterile corn oil for injections. Male or female WT and Folr1 KO mice (8 to 12 wk old) were injected intraperitoneally (i.p.) every other day for 8 d with corn oil (vehicle) or the VDR ligand, calcitriol, at a dose of 2.5 μg/kg. This dosing regimen was demonstrated to effectively elicit the desired VDR activation in vivo, while alleviating the hypercalcemic effects of calcitriol (22). At 24 h following the last injection, mice were anesthetized through isoflurane inhalation, whole blood (1 mL) was collected via cardiac puncture, and animals were decapitated prior to collection of various tissues (brain, liver, kidney, and intestine). Blood was mixed with 5 μL of EDTA (0.5 M) as an anticoagulant, and plasma was isolated following centrifugation at

1,500 × *g* for 15 min at 4 °C. All samples were stored at −80 °C until further analyzed.

Quantification of Calcium, Phosphorus, and Calcitriol in Mouse Plasma. Plasma calcium and phosphorus concentrations were measured by inductively coupled plasma atomic emission spectroscopy (Optima 7300 DV; PerkinElmer). Plasma samples were diluted 800-fold with MilliQ deionized water and filtered through a 0.22-μm filter before measurement. The emission spectra of each element were analyzed at 2 different wavelengths (calcium: 317.9 and 315.9 nm; phosphorus: 213.6 and 214.9 nm) to ensure accuracy in the measurements. Calcitriol levels in mouse plasma were measured using an enzyme immunoassay kit (catalog no. AC-62F1) manufactured by Immunodiagnostics Systems and purchased from Inter Medico.

Gene Expression Analysis. mRNA expression of specific genes of interest was quantified using qPCR. Total RNA was isolated from mouse tissues (brain capillaries, liver, kidney, and intestine) using TRIzol reagent (Invitrogen) and treated with DNase I to remove contaminating genomic DNA. RNA concentration (absorbance at 260 nm) and purity (absorbance ratio 260/280) were assessed using a Beckman Coulter DU Series 700 Scanning UV/VIS Spectrophotometer. The RNA (2 μg) was then reverse-transcribed to cDNA using a high-capacity reverse transcription cDNA kit according to the manufacturer's instructions. Specific mouse primer pairs for *Slc19a1* (RFC; Mm00446220_m1), *Slc46a1* (PCFT; Mm00546630_m1), *Folr1* (FRα; Mm00433355_m1), *Abcb1a* (P-glycoprotein [P-gp]; Mm00440761_m1), *Abcc1* (Mrp1; Mm00456156_m1), *Abcc2* (Mrp2; Mm00496899_m1), *Abcc3* (Mrp3; Mm00551550_m1), *Abcc4* (Mrp4; Mm01226381_m1), *Slc22a6* (Oat1; Mm00456258_m1), *Slc22a7* (Oat2; Mm00460672_m1), and *Slc22a8* (Oat3; Mm00459534_m1) were designed and validated by Life Technologies for use with TaqMan qPCR chemistry. All assays were performed in triplicate with the housekeeping gene for mouse cyclophilin B (Mm00478295_m1) as an internal control. For each gene of interest, the critical threshold cycle (C_T) was normalized to cyclophilin B using the comparative C_T method. The difference in C_T values (ΔC_T) between the target gene and cyclophilin B was then normalized to the corresponding ΔC_T of the vehicle control ($\Delta\Delta C_T$) and expressed as fold expression ($2^{-\Delta\Delta CT}$) to assess the relative difference in mRNA expression for each gene.

Preparation of Intravenous [$^{13}C_5$]-5-FormylTHF and Standard LC-MS/MS Solutions. Solutions for labeled and unlabeled folate calibration curves and for [$^{13}C_5$]-5-formylTHF injections were prepared by serial dilution of stock solutions according to methods described by Pfeiffer et al. (23). Spectrophotometrically validated 100 μg/mL stock solutions of the crystalline-form folates (i.e., unlabeled or [$^{13}C_5$]-labeled 5-formylTHF, 5-methylTHF, and folic acid) dissolved in phosphate buffer (pH 7.2) containing 1 g/L cysteine were aliquoted and stored at −80 °C and shielded from light until use. For intravenous (i.v.) injection, stock solutions were further diluted in sterile saline to obtain 60 μg/mL test solution.

Fourteen mixed calibrator solutions containing unlabeled and [$^{13}C_5$]-labeled 5-formylTHF and 5-methylTHF were prepared in 1% ammonium formate buffer containing 0.1% ascorbic acid. [$^{13}C_5$]-folic acid was used as an internal standard. All solutions were stored at −80 °C until LC-MS/MS analysis.

Distribution of [$^{13}C_5$]-5-FormylTHF in Mouse Plasma and Brain Tissue. [$^{13}C_5$]-5-formylTHF in sterile saline was administered to male or female WT and Folr1 KO mice (8 to 12 wk old) through i.v. injection (0.25 mg/kg of body weight) via the tail vein. Distribution of injected [$^{13}C_5$]-5-formylTHF and its metabolite [$^{13}C_5$]-5-methylTHF, as well as unlabeled 5-formylTHF and 5-methylTHF, was quantified in the collected plasma and brain tissue samples. At specific times following [$^{13}C_5$]-5-formylTHF administration, mice were anesthetized with isoflurane and whole blood (1 mL) was collected by cardiac puncture. Blood was mixed with 5 μL of EDTA (0.5 M), and plasma was isolated following centrifugation at 1,500 × *g* for 15 min at 4 °C. Plasma samples were aliquoted into tubes containing sodium ascorbate (0.5% weight/volume) to prevent folate oxidation and stored at −80 °C until LC-MS/MS analysis. Following exsanguination, brain tissues were collected, washed, and weighed before tissue processing.

Tissue Preparation for LC-MS/MS. Isolated mouse brain tissues were homogenized in Wilson–Horne buffer (2% sodium ascorbate in 50 mM Hepes, 50 mM *N*-cyclohexyl-2-aminoethanesulfonic acid, and 0.2 M 2-mercaptoethanol [pH 7.85]) and divided into 0.5-mL aliquots. Samples were then subjected to a trienzyme extraction procedure for hydrolysis of the folate polyglutamate chain (24). Briefly, a mixture of 0.5 mL of tissue extract, 0.25 mL of protease, and 1 mL of phosphate buffer (1% sodium ascorbate [pH 4.1]) was incubated at 37 °C for 2 h with gentle shaking and shielded from light. The added protease was inactivated by heating for 10 min at 100 °C and cooled on ice. Subsequently, 0.5 mL of α-amylase, 0.25 mL of rat serum conjugase, and 1 mL of phosphate buffer (1% sodium ascorbate [pH 6.8]) were added to the original mixture, and further incubated at 37 °C. After centrifugation at 5,000 × *g* for 10 min, the supernatant was collected and stored at −80 °C until further analysis.

Quantification of Plasma and Tissue [$^{13}C_5$]-5-FormylTHF or [$^{13}C_5$]-5-MethylTHF Concentrations by LC-MS/MS. Plasma and brain tissue enrichment of injected [$^{13}C_5$]-5-formylTHF or its metabolite [$^{13}C_5$]-5-methylTHF was determined by LC-MS/MS at the Analytical Facility for Bioactive Molecules (The Hospital for Sick Children), following the protocol of Pfeiffer et al. (23), with minor modifications. Before LC-MS/MS analysis, folates were extracted by solid phase extraction (SPE) from plasma samples, enzyme-digested tissues, and calibration standards. Plasma and tissue samples were first mixed with 1% ammonium formate buffer and internal standard solution (770 μL of SPE sample buffer, 275 μL of sample, and 55 μL of internal standard); calibration standards were similarly prepared (495 μL of SPE sample buffer, 275 μL of calibration solution, 55 μL of internal standard, and 275 μL of water) to give a final volume of 1.1 mL, and solutions were allowed to equilibrate at RT. SPE cartridges were conditioned with 2 mL each of acetonitrile, methanol, and 1% ammonium formate buffer (pH 3.2). One milliliter of prepared sample or calibration standards was loaded onto the cartridges and equilibrated for 1 min. The samples were then washed with 3 mL of 0.05% ammonium formate buffer containing 0.1% ascorbic acid at pH 3.4, and folates were eluted with 250 μL of elution solution (1% acetic acid, 49% water, 40% methanol, 10% acetonitrile, 0.5% ascorbic acid). Eluted samples and standards were stored in −80 °C and shielded from light until LC-MS/MS analysis.

Sample extracts (10 μL) were loaded onto a Luna C-8 analytic column for chromatographic separation using an isocratic mobile phase, as described previously (25). Mass-to-charge ratios of the transition of interest [(M + 5)] were monitored in positive ion mode via turbo ion electrospray on an AB Sciex 5500 triple-quadrupole MS system (Applied Biosystems). The concentration of each analyte in plasma or tissue samples was calculated by interpolation of the absorbed analyte/internal standard peak area ratio into the linear regression line for the calibration curve, which was obtained by plotting peak area ratios versus analyte concentrations. Brain tissue concentrations of [$^{13}C_5$]-5-formylTHF, [$^{13}C_5$]-5-methylTHF, or unlabeled 5-formylTHF and 5-methylTHF (ng/mL), as determined by LC-MS/MS, were normalized to the tissue mass and presented as nanograms per gram of tissue.

Two types of certified reference materials were employed to confirm the accuracy of the LC-MS/MS analyses. Analysis of mouse plasma was evaluated using standard reference material SRM 1955 level II (homocysteine and folate in frozen human plasma) from the National Institute of Standards and Technology (NIST). In our studies, we determined 4.30 ng/mL 5-methylTHF in the NIST 1955 plasma standard, which represents >95% of the expected value of 4.47 ± 0.11 ng/mL. We also used certified reference material BCR-487 (pig liver) from the European Commission Institute for Reference Materials and Measurements to test the accuracy of our analysis of digested mouse brain tissues and obtained an average of 104% ± 7.7 of the certified value for 5-methylTHF (n = 3 independent experiments).

Pharmacokinetic Analysis. Compartmental analyses of [$^{13}C_5$]-5-formylTHF plasma concentration-time profiles from WT mice were performed using PKsolver software for Microsoft Excel (26). Pharmacokinetic parameters were estimated after fitting the concentration data to 1- and 2-compartment models. The final model was selected based on goodness of fit through visual inspection; residual plot analysis; and statistical parameters, including weighted sum of squares, Akaike information criterion, and Schwarz criterion. Various weighting schemes (actual, estimated, 1/concentration, and 1/concentration^2) were used, and the 1/concentration^2 weighting yielded the highest model selection criterion. The area under the concentration-time curve (AUC) for plasma [$^{13}C_5$]-5-formylTHF was extrapolated to infinity ($AUC_{0\rightarrow\infty}$) and estimated using the linear trapezoidal method. The plasma terminal elimination half-life ($t_{1/2\beta}$) was determined by linear regression of the natural log-transformed concentration-time plot. Clearance (CL) and volume of distribution (V) were calculated from the equations dose/$AUC_{0\rightarrow\infty}$ and total amount of drug in body dose (mg/kg)/C_{plasma}, respectively.

Data Analysis. All experiments were repeated at least 3 times using cells from different passages or different mouse brain capillary preparations. For in vivo experiments, samples were collected from 4 to 9 animals per treatment group or time point. Results are presented as mean ± SEM. All statistical analyses were performed using Prism 6 software (GraphPad Software, Inc.). Statistical significance between 2 groups was assessed by a 2-tailed Student's t test for

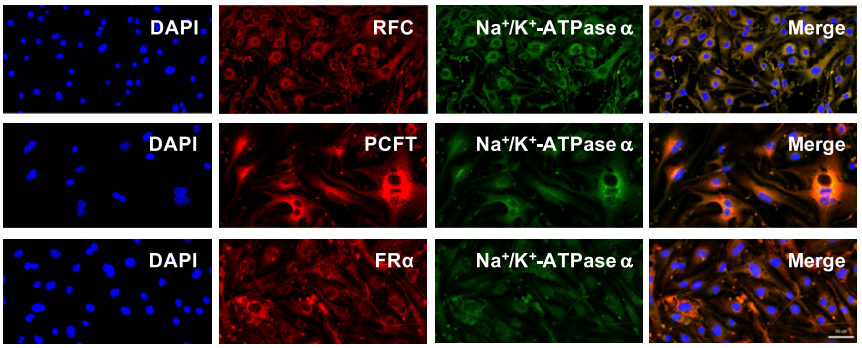

Fig. 1. Cellular localization of major folate transport pathways in primary mouse brain microvascular endothelial cells representative of the BBB. Cells were immunostained with the following: (1) DAPI nuclear marker; (2) AE390 anti-RFC (1:50), anti-HCP1/PCFT (1:50), or anti-FBP/FRα (1:50); and (3) anti-Na^+/K^+-ATPase α plasma membrane marker (1:50). Cells were visualized using confocal microscopy (LSM 700; Carl Zeiss) operated with ZEN software using a 40× or 63× objective lens. (Scale bar, 50 μm.) Three-dimensional colocalization of folate transporters/receptor and the plasma membrane marker, Na^+/K^+-ATPase α, was quantified using Imaris Bitplane software. The Pearson's coefficient values between RFC/PCFT/FRα and Na^+/K^+-ATPase α were 0.89, 0.85, and 0.68, respectively.

unpaired experimental values. Multiple group comparisons were performed using either 1-way or 2-way ANOVA with Bonferroni's post hoc test. A P value of <0.05 was considered statistically significant.

Results

Localization of Folate Receptor/Transporters in Mouse BBB. Our laboratory has previously reported robust expression of RFC, PCFT, and/FRα in several in vitro models of human and rodent BBB (14). In this study, we further investigated the cellular localization of the 3 major folate transport pathways in primary cultures of mouse brain microvascular endothelial cells by confocal microscopy (Fig. 1). RFC, PCFT, and FRα appeared to be primarily localized to the cell plasma membrane, as shown by their similar localization to the plasma membrane marker, Na^+/K^+-ATPase α. The Pearson's coefficient values between RFC/PCFT/FRα and Na^+/K^+-ATPase α were 0.89, 0.85, and 0.68, respectively, indicating robust colocalization between the folate transporters/receptor and the cell membrane marker.

Expression of Folate Receptor/Transporters in WT and Folr1 KO Mice. Relative mRNA expression of major folate transport pathways was determined in WT and Folr1 KO mouse tissues by qPCR (Fig. 2). We confirmed that *Folr1* (FRα) mRNA was not present in various tissues (isolated brain capillaries, liver, and kidney) of Folr1 KO mice compared with WT controls. We also did not observe significant differences in the level of *Slc19a1* (RFC) and *Slc46a1* (PCFT) expression between Folr1 KO and WT animals, suggesting a lack of compensation from these transporters in response to the loss of FRα.

Effect of Calcitriol on RFC Expression in WT and Folr1 KO Mice. To examine the effect of VDR activation in the regulation of RFC in vivo, mice were treated i.p. with the VDR ligand, calcitriol [$1,25(OH)_2D_3$; 2.5 μg/kg] every other day for 8 d. Significant increases in *Slc19a1* (RFC) mRNA were observed in isolated brain capillaries (1.5-fold), liver (2-fold), kidney (1.3-fold), and duodenum (6-fold) of WT or Folr1 KO animals compared with vehicle (Figs. 3*A* and 4*A*). We additionally used P-gp as a positive control since the functional expression of this membrane transporter has been extensively demonstrated to be regulated by VDR (27, 28). As shown in Figs. 3*B* and 4*B*, *Abcb1a* (P-gp) mRNA levels were significantly elevated in various tissues of WT and Folr1 KO mice following calcitriol treatment. A modest but significant increase in *Slc46a1* (PCFT) mRNA expression was also observed in isolated brain capillaries (1.5-fold) and liver (1.4-fold) of calcitriol-treated WT mice; however the contribution of this transporter in mediating folate delivery at the BBB may be less relevant due to the low pH required for optimal PCFT activity (*SI Appendix*, Fig. S1). Furthermore, mRNA expression of several members of the organic anion transporter (OAT) and multidrug resistance-associated protein (MRP) families were determined following calcitriol treatment (*SI Appendix*, Fig. S2). A number of these membrane-associated transporters exhibit relatively modest affinities for folates (OAT1–3, K_m = 10 to 700 μM; MRP1–4, K_m = 0.2 to 2 mM) and could potentially contribute to the observed effect of calcitriol on brain folate levels. Significant induction in *Slc22a8* (Oat3) and *Abcc3* (Mrp3) mRNA was observed in kidney tissues of calcitriol-treated WT and Folr1 KO mice compared with vehicle (*SI Appendix*, Fig. S2*A*). *Abcc2*

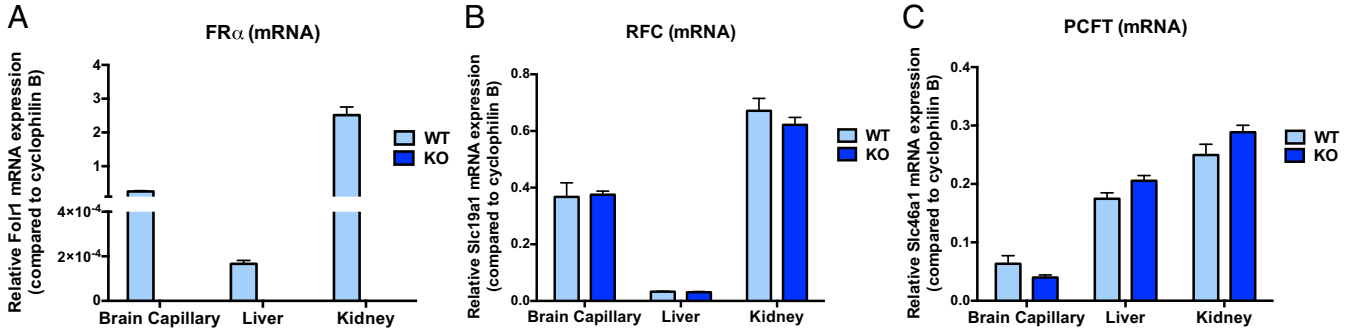

Fig. 2. Relative expression of major folate transport pathways in various tissues of WT and Folr1 KO mice. mRNA expression of mouse *Folr1* (*A*, FRα), *Slc19a1* (*B*, RFC), and *Slc46a1* (*C*, PCFT) genes was determined using TaqMan gene expression assay. Results are presented as mean relative mRNA expression ± SEM normalized to the housekeeping mouse cyclophilin B gene from n = 3 independent experiments (total of 8 animals per group).

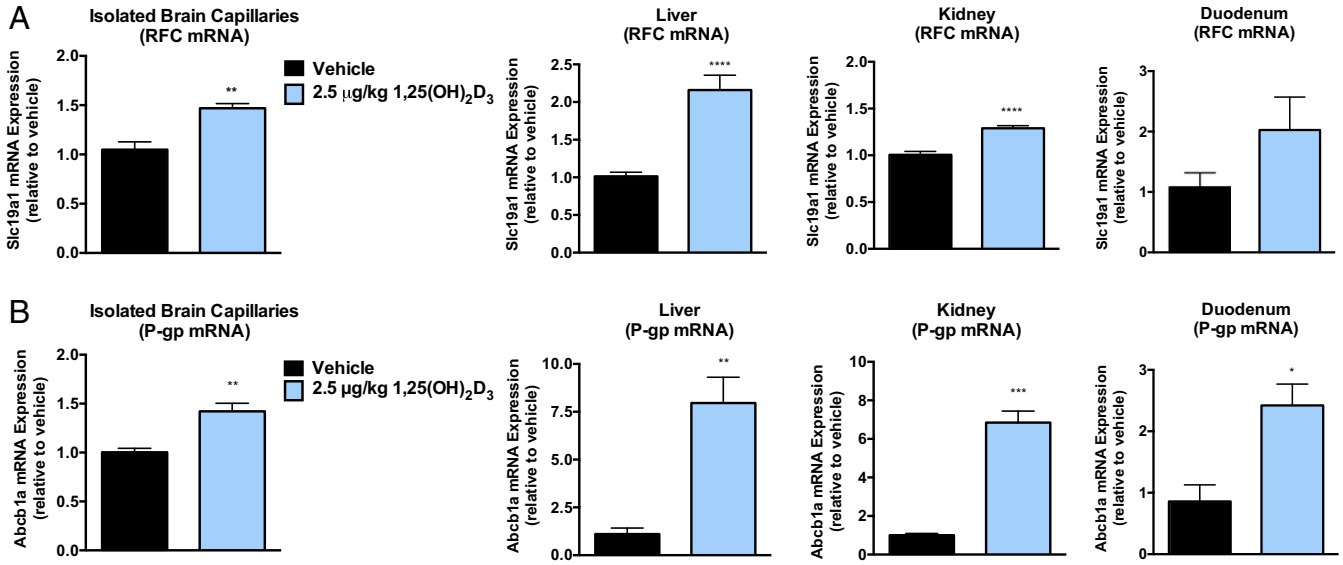

Fig. 3. Effect of calcitriol treatment on RFC and P-gp expression in WT mice. Significant increases in *Slc19a1* (*A*, RFC) and *Abcb1a* (*B*, P-gp) mRNA were observed in isolated brain capillaries, liver, kidney, and/or duodenum of mice treated with calcitriol (2.5 μg/kg) compared with vehicle (corn oil). Results are presented as mean ± SEM for $n = 3$ independent experiments (total of 8 to 9 animals per group). Asterisks represent data points significantly different from vehicle (*$P < 0.05$; **$P < 0.01$; ***$P < 0.001$; ****$P < 0.0001$).

(Mrp2) mRNA was also increased in the liver of WT and Folr1 KO mice following calcitriol administration (*SI Appendix*, Fig. S2*B*). No significant changes in Oat or Mrp mRNA expression was observed in mouse brain capillaries isolated from vehicle and calcitriol-treated WT and Folr1 KO animals (*SI Appendix*, Fig. S2*C*).

Systemic Effects of Calcitriol Treatment. The body weight of WT and Folr1 KO mice was also monitored prior to and during calcitriol treatments. Changes in body weight relative to day 0 (time before vehicle/calcitriol injections; initial weight set to 1) was plotted over a course of 6 d (Fig. 5*A*). WT and Folr1 KO mice treated with calcitriol showed a statistically significant decrease in body weight (~10%) starting at day 4 compared with vehicle control. However, this observed weight loss plateaued after prolonged calcitriol administration (i.e., 16 d) (*SI Appendix*, Fig. S3). Since vitamin D is involved in numerous physiological processes, particularly calcium uptake and bone metabolism, we also determined plasma levels of calcium and phosphorus in response to calcitriol administration. As shown in Fig. 5 *B* and *C*, the 8-d treatment regimen significantly increased calcitriol (5.5-fold) and calcium (1.5-fold) concentrations

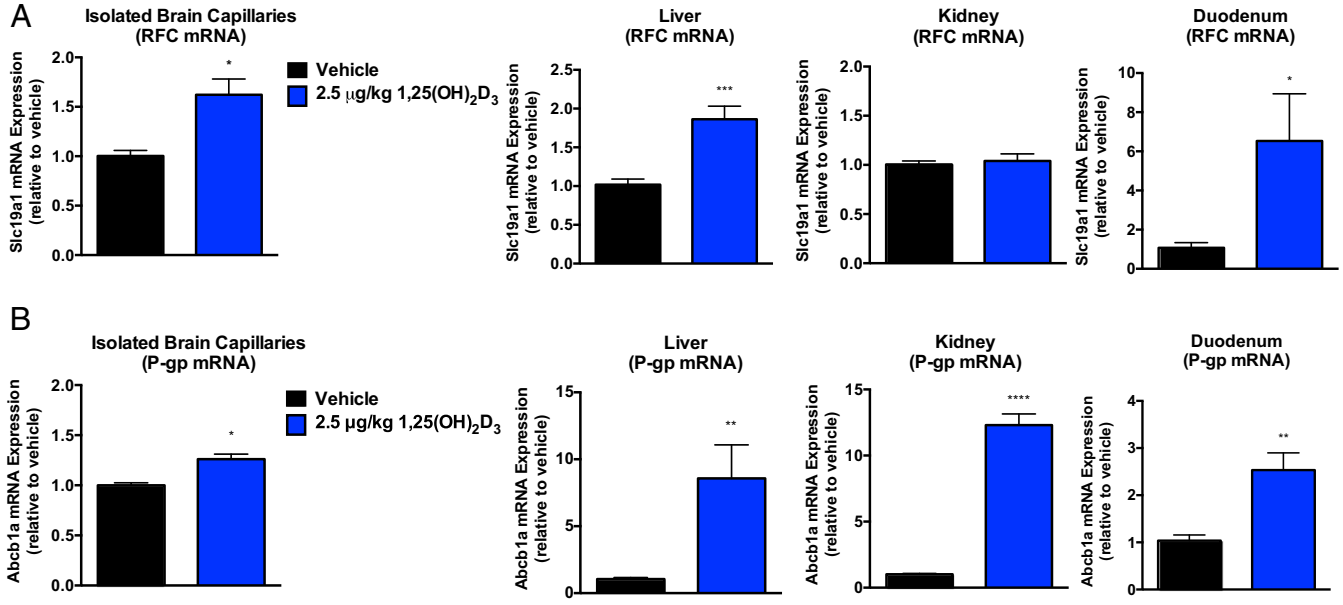

Fig. 4. Effect of calcitriol treatment on RFC and P-gp expression in Folr1 KO mice. Significant increases in *Slc19a1* (*A*, RFC) and *Abcb1a* (*B*, P-gp) mRNA were observed in isolated brain capillaries, liver, duodenum, and/or kidney of mice treated with calcitriol (2.5 μg/kg) compared with vehicle (corn oil). Results are presented as mean ± SEM for $n = 3$ independent experiments (total of 8 to 9 animals per group). Asterisks represent data points significantly different from vehicle (*$P < 0.05$; **$P < 0.01$; ***$P < 0.001$; ****$P < 0.0001$).

in mouse plasma. Phosphorus levels, on the other hand, remained unchanged following calcitriol treatment (Fig. 5*D*).

Assessment of Folate Levels (5-FormylTHF and 5-MethylTHF) in WT and Folr1 KO Mice. Basal levels of reduced folates, 5-formylTHF and 5-methylTHF, were initially determined in plasma and brain tissues of WT and Folr1 KO mice by LC-MS/MS, respectively (Fig. 6). We confirmed that the concentrations of 5-formylTHF and 5-methylTHF in the plasma (C_{plasma}) and brain (C_{brain}) of Folr1 KO mice were much lower than in WT animals, suggesting that loss of Folr1 adversely affects folate uptake to the brain as well as folate conservation in the body, which primarily occurs via Folr1-mediated reabsorption in the kidneys.

Plasma and Tissue Distribution of [$^{13}C_5$]-5-FormylTHF in WT Mice. In vivo transport activity of RFC was examined using [$^{13}C_5$]-5-formylTHF, which is a heavy isotope tracer that can be used to evaluate folate distribution in WT and/or Folr1 KO mice. 5-formylTHF (leucovorin or folinic acid) is a known RFC substrate (K_m = 2 to 7 μM) and a stable form of folate primarily used in the treatment of neurodevelopmental disorders, such as hereditary folate malabsorption and cerebral folate deficiency syndrome. Plasma or serum distribution of injected [$^{13}C_5$]-5-formylTHF was previously characterized in human subjects (25, 29), but its distribution to biological tissues has yet to be examined. To determine whether [$^{13}C_5$]-5-formylTHF can successfully penetrate across the BBB, a single bolus dose of [$^{13}C_5$]-5-formylTHF (0.25 mg/kg) was initially administered to WT mice through i.v. injection via the tail vein. As shown in Fig. 7*A*, the amount of [$^{13}C_5$]-5-formylTHF in WT plasma rose to a maximum concentration of 403 ± 150 ng/mL after i.v. injection, followed by a rapid decline to baseline at 30 to 120 min postinjection. Fitting of plasma [$^{13}C_5$]-5-formylTHF concentration data to a 2-compartment i.v. bolus model also yielded the following pharmacokinetic parameter estimates: $t_{1/2\beta}$ = 25.01 min, V = 396.34 mL/kg, $AUC_{0\rightarrow\infty}$ = 2,849 ng·min·mL^{-1}, and

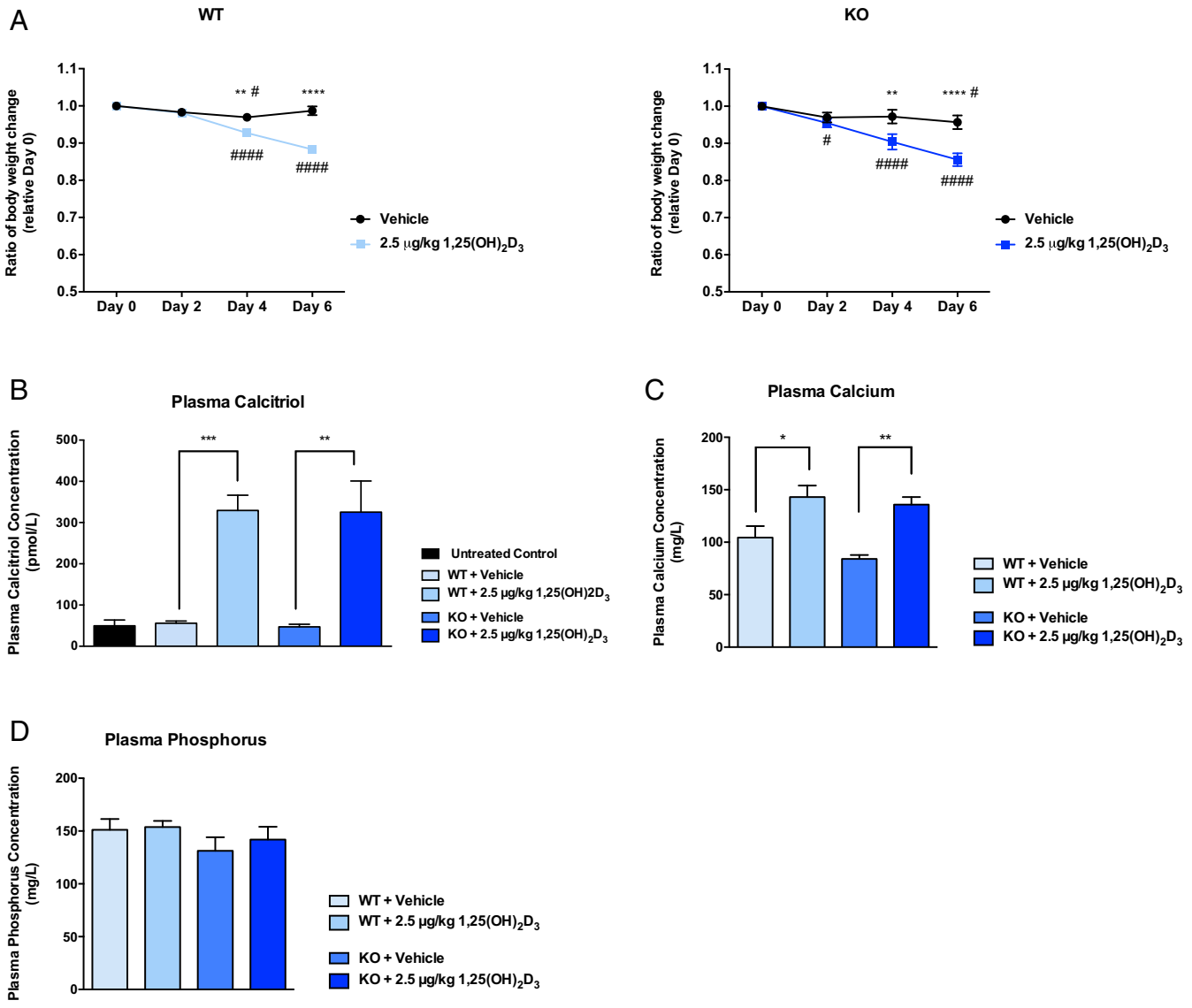

Fig. 5. Effect of calcitriol treatment on body weight, plasma calcitriol, calcium, and phosphorus in WT and Folr1 KO mice. (*A*) Significant weight loss was observed at days 4 and 6 following treatment with calcitriol (2.5 μg/kg) compared with vehicle (corn oil). Calcitriol treatment also increased calcitriol (*B*) and calcium (*C*) concentrations in mouse plasma, but not phosphorus (*D*). Results are presented as mean ± SEM for n = 3 independent experiments, with at least 4 animals per group. Asterisks represent data points significantly different from vehicle control (*P < 0.05; **P < 0.01; ***P < 0.001; ****P < 0.0001). For weight data, the pound symbol represents data points significantly different from day 0 (time before vehicle or calcitriol injections) ($^{\#}P$ < 0.05; $^{\#\#\#\#}P$ < 0.0001).

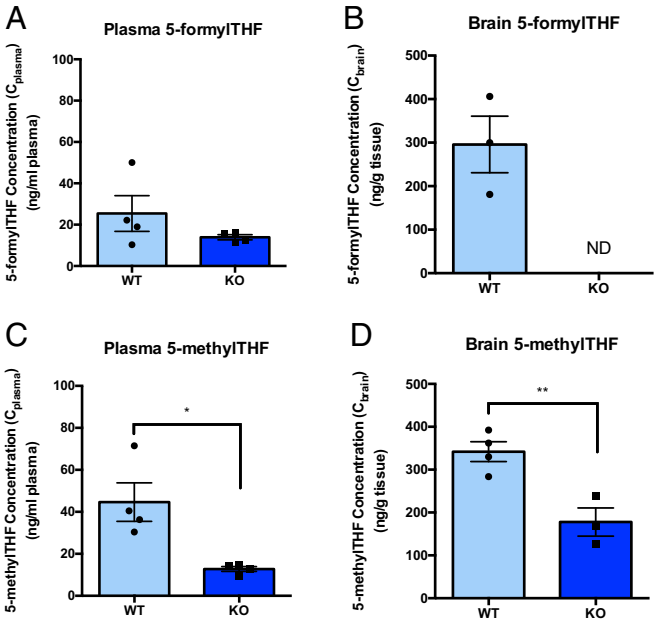

Fig. 6. Basal folate levels in WT versus Folr1 KO mice. Plasma and brain concentrations of unlabeled 5-formylTHF (*A* and *B*) and 5-methylTHF (*C* and *D*) were much lower in Folr1 KO mice compared with WT mice. ND, 5-formylTHF levels in brain tissues of Folr1 KO mice were not detected by LC-MS/MS. Results are presented as mean ± SEM (total of 4 animals per group). Asterisks represent data points significantly different from WT (*P < 0.05; **P < 0.01).

CL = 87.76 mL·min^{-1}·kg^{-1} (*SI Appendix*, Table S1). Furthermore, plasma levels of [$^{13}C_5$]-5-methylTHF, a metabolite of [$^{13}C_5$]-5-formylTHF and the major circulating form of folates, was measured to assess the conversion between different folate forms. As shown in Fig. 7*A*, a steady increase in plasma [$^{13}C_5$]-5-methylTHF was observed following [$^{13}C_5$]-5-formylTHF administration, which then declined toward baseline at 60 min postinjection. Most importantly, the presence of both folate forms was also detected in brain tissues isolated from treated animals, with [$^{13}C_5$]-5-methylTHF being present at higher concentrations over the 120-min study period compared with [$^{13}C_5$]-5-formylTHF (Fig. 7*B*).

Effect of Calcitriol Treatment on Plasma and Tissue Distribution of [$^{13}C_5$]-5-FormylTHF in Folr1 KO Mice. To determine whether in vivo activation of VDR through calcitriol treatment will result in an increase in RFC functional activity, Folr1 KO mice were pretreated with calcitriol (2.5 μg/kg) or vehicle (corn oil) every other day for 8 d. At 24 h following the last calcitriol dose, each mouse received a single bolus dose of [$^{13}C_5$]-5-formylTHF (0.25 mg/kg) by tail vein injection and was subsequently euthanized 5 min postinjection. As shown in Fig. 8*A*, plasma levels of injected [$^{13}C_5$]-5-formylTHF (C_{plasma}) did not differ between the 4 treatment groups: (1) untreated WT mice, (2) untreated Folr1 KO mice, (3) vehicle-treated Folr1 KO mice, and (4) calcitriol-treated Folr1 KO mice. We also found that brain concentrations of [$^{13}C_5$]-5-formylTHF (C_{brain}) were lower in Folr1 KO animals (untreated and vehicle-treated) compared with WT controls, suggesting inefficient folate uptake to the brain with the loss of Folr1 (Fig. 8*B*). However, pretreatment with calcitriol resulted in over a 6-fold increase in [$^{13}C_5$]-5-formylTHF accumulation in brain tissues of Folr1 KO mice compared with vehicle. In fact, the levels of [$^{13}C_5$]-5-formylTHF found in brain tissues of calcitriol-treated Folr1 KO mice were remarkably comparable to those of WT mice (Fig. 8*B*). We also determined brain-to-plasma concentration ratios (C_{brain}/C_{plasma}) of injected [$^{13}C_5$]-5-formylTHF to evaluate brain penetration of this compound (Fig. 8*C*). As expected, much lower C_{brain}/C_{plasma} ratios were observed in Folr1 KO mice (untreated and vehicle-treated) compared with WT controls, and pretreatment with calcitriol significantly increased the C_{brain}/C_{plasma} ratio of injected [$^{13}C_5$]-5-formylTHF by ∼15-fold. Taken together, these results demonstrate a significant and robust enhancement of RFC-mediated brain folate uptake in Folr1 KO mice following VDR activation with calcitriol.

Discussion

Folates are essential for proper cognitive function, especially during rapid periods of growth and brain development in infancy and childhood. Folate deficiency has been implicated in a number of neurodevelopmental disorders. Low maternal folate status is an

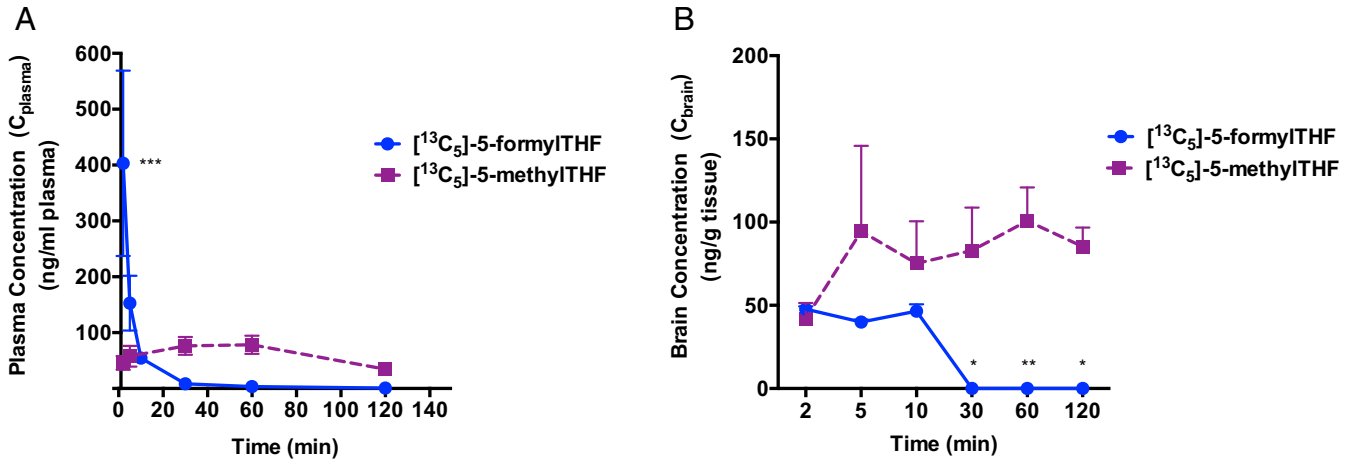

Fig. 7. Plasma and brain distribution of [$^{13}C_5$]-5-formylTHF and its metabolite [$^{13}C_5$]-5-methylTHF in WT mice. Plasma (*A*, ng/mL) and brain tissue (*B*, ng/g) concentrations were measured over 120 min following an i.v. bolus injection of 0.25 mg/kg [$^{13}C_5$]-5-formylTHF in WT mice. Results are presented as mean ± SEM for each time point (total of 4 animals per time point). Plasma [$^{13}C_5$]-5-formylTHF data were fitted to a 2-compartment i.v. bolus pharmacokinetic model. The change in plasma [$^{13}C_5$]-5-formylTHF concentration over 120 min following i.v. injection was statistically significant (P < 0.001), but the change in plasma [$^{13}C_5$]-5-methylTHF was not. The change in brain [$^{13}C_5$]-5-formylTHF or [$^{13}C_5$]-5-methylTHF concentrations over the 120-min study period was not statistically significant. Asterisks represent significant differences between [$^{13}C_5$]-5-formylTHF and [$^{13}C_5$]-5-methylTHF concentrations in plasma or brain tissue for each time point (*P < 0.05; **P < 0.01; ***P < 0.001).

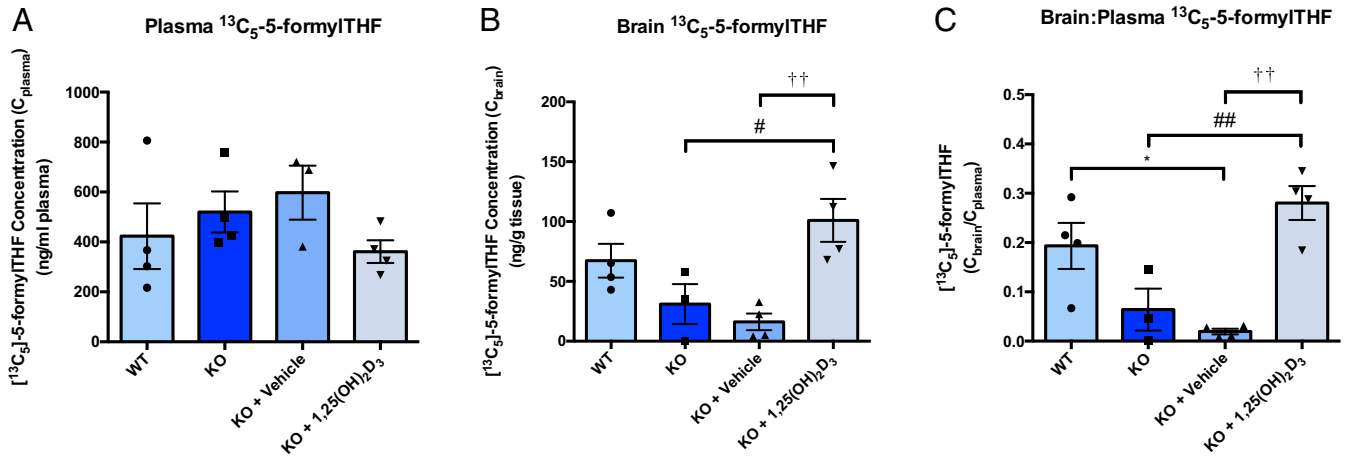

Fig. 8. Effect of calcitriol treatment on plasma and brain distribution of [$^{13}C_5$]-5-formylTHF in Folr1 KO mice. Plasma (*A*, ng/mL) and brain tissue (*B*, ng/g) concentrations were measured over 5 min following an i.v. bolus injection of 0.25 mg/kg [$^{13}C_5$]-5-formylTHF to WT and Folr1 KO mice. (*C*) Tissue-to-plasma (C_{brain}/C_{plasma}) concentration ratio of injected [$^{13}C_5$]-5-formylTHF was also determined. Results are presented as mean ± SEM (total of 4 animals per group). Asterisk, pound, and dagger symbols represent data points significantly different from untreated WT, untreated Folr1 KO, and vehicle-treated Folr1 KO groups, respectively (*$P < 0.05$; $^{\#}P < 0.05$; $^{\#\#}P < 0.01$; $^{\dagger\dagger}P < 0.01$).

important contributor to the prevalence of congenital malformations like neural tube defects (30). Abnormalities in folate transport have also been associated with hereditary folate malabsorption (8), cerebral folate deficiency syndrome (10), and autism spectrum disorders (31). Several lines of evidence indicate that folate supplementation can somewhat reduce the occurrence of these neurological disorders; however, current therapeutic approaches are not sufficiently effective (8, 32, 33).

There are 2 potential routes for folate delivery into the brain: (1) the blood–CSF barrier at the choroid plexus and (2) the cerebral vasculature endothelium or BBB. As previously indicated, brain folate transport primarily occurs at the choroid plexus via FRα and PCFT (7, 8). Loss of FRα or PCFT function can severely impair folate uptake into the CSF, causing neural folate deficiency that manifests into childhood neurodegenerative disorders, such as cerebral folate deficiency (9, 10) and hereditary folate malabsorption (4, 8), respectively. These 2 disorders share similar neurological symptoms, but with distinct clinical presentations. Hereditary folate malabsorption occurs within a few months of birth and is characterized by defective intestinal folate absorption causing systemic folate deficiency, as well as impaired brain folate transport resulting in low CSF folate (4, 8). On the other hand, patients with cerebral folate deficiency exhibit normal blood folate levels and only present with neurological deficits after 2 to 3 y of age (9, 10).

The vascular BBB represents an arterial route for brain folate transport, although the exact mechanisms of folate uptake at this site remain unknown (15–17). There is some clinical evidence pertaining to the role of the BBB in folate delivery. In particular, some patients with hereditary folate malabsorption can present with mild neurological deficits despite suboptimal CSF folate levels, suggesting that in the absence of choroid plexus function, brain folate uptake can still occur via the BBB; however, the efficiency of transport varies among patients. Furthermore, the earlier onset of hereditary folate malabsorption compared with cerebral folate deficiency could be due to the presence of severe systemic folate deficiency, which may limit the protective effect of BBB folate transport (8). In contrast, despite normal systemic folate levels in individuals with cerebral folate deficiency and presumed normal folate uptake at the BBB, the loss of FRα function still results in low CSF folate levels ultimately causing cognitive deficits. These clinical observations suggest that folate transport across the BBB may not adequately supply neural cells with sufficient folates to sustain normal development (34, 35). Thus, modulating folate transport at the level of the BBB could significantly contribute to folate uptake into the CNS.

Finding new approaches for enhancing brain folate delivery may have a significant impact on the treatment of childhood neurometabolic disorders caused by folate deficiency. Our group has reported that the vascular BBB could present an alternative route for brain folate transport, especially when inactivation of FRα or PCFT impairs the major route of folate uptake at the choroid plexus (14). We further demonstrated in vitro that functional expression of another folate transporter, RFC, and its upregulation by the VDR nuclear receptor could potentially increase folate transport across the BBB (14). In the present study, we go on to demonstrate in vivo that loss of Folr1 expression results in a substantial decrease in the delivery of $^{13}C_5$-folates to the brain and that delivery is restored by administration of the VDR-activating ligand, calcitriol. The data indicate that this is due to the salutary impact of calcitriol on the expression of RFC at the BBB. Since Folr1 is almost exclusively expressed in the choroid plexus, these findings (1) represent a demonstration of the substantial impact of the loss of choroid plexus function on the delivery of folates to the brain, as observed in hereditary folate malabsorption and cerebral folate deficiency syndrome, and (2) suggest a novel adjunct therapy to the treatment of these neurological disorders with calcitriol.

Using immunocytochemical staining and confocal microscopy, we characterized the localization of RFC, PCFT, and FRα in primary mouse microvessel endothelial cells representative of an in vitro BBB system (Fig. 1). We confirmed that all 3 folate transport pathways were primarily localized to the plasma membrane, as evident by their similar localization to the plasma membrane marker Na^+/K^+-ATPase α. Detection of robust expression of folate transporters at the mouse BBB corroborates previous reports (14, 16, 36) and provides evidence of a potential role for the BBB in brain folate delivery.

To assess the contribution of folate transporters (i.e., RFC) in facilitating folate uptake across the BBB, we implemented the use of an in vivo mouse model lacking Folr1 (Folr1 KO). Systemic deletion of this receptor was confirmed through qPCR analysis, which showed a lack of *Folr1* (FRα) mRNA expression in various tissues (liver, kidney, and isolated brain capillaries representative of the BBB) of Folr1 KO mice compared with WT controls (Fig. 2). We also did not observe significant differences

in the level of *Slc19a1* (RFC) and *Slc46a1* (PCFT) expression between Folr1 KO and WT animals, indicating a lack of compensation from these transporters in response to the loss of Folr1. Given these findings, it is important to note that although PCFT was detected in isolated mouse brain capillaries, this transporter may not be functionally relevant at this site due to the neutral pH of the BBB interface and the low pH required for optimal PCFT uptake. Thus, our subsequent studies focused on characterizing the role of RFC at the level of the BBB.

In vivo regulation of RFC by VDR was examined through i.p. administration of the VDR ligand, calcitriol, to WT and Folr1 KO mice using the dosing regimen specified by Chow et al. (22). We demonstrated that calcitriol treatment significantly increased *Slc19a1* (RFC) mRNA expression in isolated brain capillaries (1.5-fold) of WT and Folr1 KO mice (Figs. 3*A* and 4*A*). These results are in agreement with our laboratory's previous findings that in vitro exposure of hCMEC/D3 cells and mouse brain capillaries to calcitriol resulted in over 50% upregulation of RFC mRNA and protein (14). In the present study, *Slc19a1* (RFC) mRNA was also induced in other tissues known to express this transporter, such as the liver (2-fold), kidney (1.3-fold), or duodenum (6-fold) (Figs. 3*A* and 4*A*). Only a modest increase in *Slc46a1* (PCFT) mRNA was observed in isolated brain capillaries (1.5-fold) and liver (1.4-fold) of calcitriol-treated WT mice, but the contribution of this transporter in BBB folate delivery may be less relevant due to the low pH required for optimal PCFT activity (*SI Appendix*, Fig. S1). Furthermore, *Abcb1a* (P-gp) mRNA was elevated in various tissues of WT and Folr1 KO mice following calcitriol treatment (Figs. 3*B* and 4*B*). This was not surprising since VDR is a key regulator of a number of membrane transporters, including the drug efflux pump, P-gp (28, 37). However, induction of this transporter at the BBB may have functional consequences since P-gp has also been identified to be a low-affinity efflux transporter of folates (K_m = 0.2 to 2 mM) and could potentially oppose folate uptake by RFC (38). We further examined the expression of several OAT and MRP transporters that are known to transport folates (OAT1–3, K_m = 10 to 700 μM; MRP1–4, K_m = 0.2 to 2 mM) and potentially contribute to the observed effect of calcitriol on brain folate levels. As shown in *SI Appendix*, Fig. S2, substantial increases in *Slc22a8* (Oat3), *Abcc2* (Mrp2), or *Abcc3* (Mrp3) mRNA were observed in kidney or liver tissues of calcitriol-treated mice, but not in isolated mouse brain capillaries. These results suggest that there may be minimal contribution from these transporters in folate uptake at the BBB, further supporting our hypothesis that folate transport at the BBB could be largely mediated by RFC.

Systemic effects of calcitriol administration were also investigated to evaluate the safety of our treatment protocol. As expected, exogenous administration of calcitriol significantly increased calcitriol levels in plasma of treated mice (5.5-fold) as seen in earlier reports by other groups (39) (Fig. 5*B*). The alternate-day dosing regimen recommended by Chow et al. (22) was also shown previously to alleviate the hypercalcemic and weight loss effects of calcitriol, but we observed significant increases in plasma calcium concentrations (1.5-fold) of WT and Folr1 KO mice after the 8-d treatment period in our studies (Fig. 5*C*). Phosphorus levels, on the other hand, were unchanged following calcitriol treatment (Fig. 5*D*). WT and Folr1 KO mice also exhibited a statistically significant decrease in body weight starting at day 4 of calcitriol injections (Fig. 5*A*), but this weight loss plateaued after prolonged calcitriol administration (*SI Appendix*, Fig. S3). Hypercalcemia may have been induced by VDR-mediated transactivation of calcium ion channels in the kidney and intestine (i.e., TRPV5, TRPV6), resulting in volume depletion due to frequent urination (39). Although the observed hypercalcemia and weight loss did not seem to affect the animals' overall health, exogenous administration of calcitriol still requires strict monitoring to avoid toxicities associated with VDR activation in vivo. Supplementation with other vitamin D forms, such as ergocalciferol and cholecalciferol, may also be helpful in reducing toxicities since these compounds require initial conversion into the active calcitriol form by CYP27B1, an enzyme tightly regulated by serum calcium levels (40).

Folate distribution in WT and Folr1 KO mice was subsequently examined to further understand the effect of VDR activation on RFC functional activity, particularly at the BBB. We initially determined that basal concentrations of reduced folates, 5-formylTHF and 5-methylTHF, in the plasma (C_{plasma}) and brain (C_{brain}) of Folr1 KO mice were much lower compared with WT mice (Fig. 6). These results suggest that despite supplementing with high doses of folic acid (40 mg/kg) during gestation, loss of Folr1 function continues to affect brain folate uptake as well as folate reabsorption in the kidneys of adult Folr1 KO animals (41). We also used [$^{13}C_5$]-labeled 5-formylTHF to evaluate folate disposition in vivo. In our hands, i.v. administration of [$^{13}C_5$]-5-formylTHF in WT mice yielded pharmacokinetic parameters that are comparable to those in an earlier report by Wu and Pardridge (17) (Fig. 7*A* and *SI Appendix*, Table S1). Significant levels of injected [$^{13}C_5$]-5-formylTHF and its metabolite, [$^{13}C_5$]-5-methylTHF, were also detected in brain tissues of WT mice, consistent with transport of [$^{13}C_5$]-labeled folates across the BBB (Fig. 7*B*). Finally, to verify whether VDR activation will also induce RFC function in vivo, Folr1 KO mice were subjected to an 8-d pretreatment with calcitriol or vehicle before receiving a single i.v. injection of [$^{13}C_5$]-5-formylTHF. Within the Folr1 KO brain tissues, we observed a significant and remarkable increase of [$^{13}C_5$]-5-formylTHF concentrations (6-fold) and corresponding C_{brain}/C_{plasma} ratio (15-fold) in calcitriol-treated mice compared with the vehicle-treated group (Fig. 8). These findings are most exciting as they demonstrate that in vivo induction of RFC functional expression through activation of VDR by calcitriol can significantly increase brain folate delivery in Folr1 KO mice. In fact, pretreatment with calcitriol resulted in brain [$^{13}C_5$]-5-formylTHF levels that were comparable to those of WT animals, suggesting that upregulation of RFC could potentially compensate for the loss of Folr1-mediated brain folate uptake.

Beyond abnormalities in folate delivery to the brain due to loss-of-function mutations in FRα and PCFT, low CSF folate level was previously identified in at least 2 types of autism spectrum disorders, such as Rett syndrome and infantile low-functioning autism (42, 43). Reduced brain folate transport was linked to the presence of FRα autoantibodies, which inhibit FRα function either by blocking folate binding to the receptor or by binding to an epitope distant from the folate-binding site and disrupting receptor function. A high prevalence of FRα autoantibodies (75%) was also reported in a cohort of children with idiopathic autism spectrum disorders and was found to correlate with low folate concentrations in the CSF (31). The intervention with 5-formylTHF (leucovorin or folinic acid) has shown favorable responses in autism spectrum disorders, especially among patients who are positive for FRα autoantibodies. Ramaekers et al. (42) reported partial recovery of neurological and social impairments in patients with infantile low-functioning autism after oral supplementation with 5-formylTHF. Frye et al. (31) also observed marked improvements in attention, language, and behavior in over 60% of patients treated with high oral doses of 5-formylTHF compared with nontreated controls. In a randomized, double-blind, placebo-controlled trial conducted by the same group, 12-wk high-dose oral 5-formylTHF supplementation significantly improved verbal communication in patients expressing FRα autoantibodies (44). Despite the promising effects of 5-formylTHF intervention in autism spectrum disorders, there is still a need to establish more effective therapies. Frye et al. (31) have reported that prolonged intake of 5-formylTHF at such high doses could result in adverse events, including insomnia, gastroesophageal reflux, and worsening aggression. Since autism is a lifelong disorder, finding an optimal therapeutic approach

with limited adverse effects is important. Our present findings could potentially represent a new strategy for enhancing folate delivery to the brain via RFC at the BBB.

In summary, we have shown in vivo that loss of Folr1 substantially decreases folate delivery to the brain, demonstrating the major contribution of the choroid plexus to brain folate transport. We further provide evidence that in vivo activation of VDR by its natural activating ligand, calcitriol, can induce RFC expression in mice lacking Folr1. These findings suggest that augmenting RFC functional expression enhances folate delivery at the BBB and could potentially compensate for the loss of FRα-mediated folate uptake at the choroid plexus. The current therapeutic approach for neurological disorders resulting from folate transport defects is to achieve high 5-formylTHF blood levels in order to deliver sufficient folate to the brain to sustain normal neural development. However, despite achievement of high blood folate levels, CSF folate levels are still below the normal range and neurological signs, particularly seizures, may be difficult to control (8, 32, 45, 46). Therefore, modulating folate transport at the BBB through RFC offers a therapeutic approach to improving brain folate delivery for the treatment of neurometabolic disorders caused by loss of FRα or PCFT function.

ACKNOWLEDGMENTS. We thank Dr. Robert Steinfeld (Department of Pediatric Neurology, University Children's Hospital Zürich, Zürich, Switzerland) for his initial insights on this work. We acknowledge Dr. Bogdan Wlodarczyk (Baylor College of Medicine, Houston, TX) for his excellent advice on establishing the animal breeding colonies. We also thank Adrian Turner for his assistance with the isolation of mouse brain capillaries. This research was supported by an operating grant from the Natural Sciences and Engineering Research Council of Canada (NSERC Grant 498383 to R.B.). C.A. was a recipient of an internal graduate fellowship and Centre for Pharmaceutical Oncology scholarship from the Leslie Dan Faculty of Pharmacy (University of Toronto). R.H.F. was supported by NIH Grants R01HD081216 and R01HD083809. I.D.G. was supported by National Cancer Institute Grant CA082621. D.L.O. was supported by NSERC Grant 43302.

1. A. S. Tibbetts, D. R. Appling, Compartmentalization of mammalian folate-mediated one-carbon metabolism. *Annu. Rev. Nutr.* **30**, 57–81 (2010).
2. B. A. Kamen, A. K. Smith, A review of folate receptor alpha cycling and 5-methyltetrahydrofolate accumulation with an emphasis on cell models in vitro. *Adv. Drug Deliv. Rev.* **56**, 1085–1097 (2004).
3. H. Elnakat, M. Ratnam, Distribution, functionality and gene regulation of folate receptor isoforms: Implications in targeted therapy. *Adv. Drug Deliv. Rev.* **56**, 1067–1084 (2004).
4. A. Qiu *et al*., Identification of an intestinal folate transporter and the molecular basis for hereditary folate malabsorption. *Cell* **127**, 917–928 (2006).
5. M. Visentin, N. Diop-Bove, R. Zhao, I. D. Goldman, The intestinal absorption of folates. *Annu. Rev. Physiol.* **76**, 251–274 (2014).
6. R. Zhao, I. D. Goldman, Folate and thiamine transporters mediated by facilitative carriers (SLC19A1-3 and SLC46A1) and folate receptors. *Mol. Aspects Med.* **34**, 373–385 (2013).
7. M. Grapp *et al*., Choroid plexus transcytosis and exosome shuttling deliver folate into brain parenchyma. *Nat. Commun.* **4**, 2123 (2013).
8. R. Zhao, S. Aluri, I. D. Goldman, The proton-coupled folate transporter (PCFT-SLC46A1) and the syndrome of systemic and cerebral folate deficiency of infancy: Hereditary folate malabsorption. *Mol. Aspects Med.* **53**, 57–72 (2017).
9. M. Grapp *et al*., Molecular characterization of folate receptor 1 mutations delineates cerebral folate transport deficiency. *Brain* **135**, 2022–2031 (2012).
10. R. Steinfeld *et al*., Folate receptor alpha defect causes cerebral folate transport deficiency: A treatable neurodegenerative disorder associated with disturbed myelin metabolism. *Am. J. Hum. Genet.* **85**, 354–363 (2009).
11. V. T. Ramaekers *et al*., Autoantibodies to folate receptors in the cerebral folate deficiency syndrome. *N. Engl. J. Med.* **352**, 1985–1991 (2005).
12. G. Benoit *et al*., International union of pharmacology. LXVI. Orphan nuclear receptors. *Pharmacol. Rev.* **58**, 798–836 (2006).
13. J. J. Eloranta *et al*., Vitamin D3 and its nuclear receptor increase the expression and activity of the human proton-coupled folate transporter. *Mol. Pharmacol*. **76**, 1062–1071 (2009). Erratum in: *Mol. Pharmacol.* 77, 885 (2010).
14. C. Alam, M. T. Hoque, R. H. Finnell, I. D. Goldman, R. Bendayan, Regulation of reduced folate carrier (RFC) by vitamin D receptor at the blood-brain barrier. *Mol. Pharm.* **14**, 3848–3858 (2017).
15. J. R. Araújo, P. Gonçalves, F. Martel, Characterization of uptake of folates by rat and human blood-brain barrier endothelial cells. *Biofactors* **36**, 201–209 (2010).
16. Y. Wang, R. Zhao, R. G. Russell, I. D. Goldman, Localization of the murine reduced folate carrier as assessed by immunohistochemical analysis. *Biochim. Biophys. Acta* **1513**, 49–54 (2001).
17. D. Wu, W. M. Pardridge, Blood-brain barrier transport of reduced folic acid. *Pharm. Res.* **16**, 415–419 (1999).
18. G. N. Chan, R. E. Cannon, Assessment of ex vivo transport function in isolated rodent brain capillaries. *Curr. Protoc. Pharmacol* **76**, 7.16.1–7.16.16 (2017).
19. M. T. Hoque, K. R. Robillard, R. Bendayan, Regulation of breast cancer resistant protein by peroxisome proliferator-activated receptor α in human brain microvessel endothelial cells. *Mol. Pharmacol.* **81**, 598–609 (2012).
20. J. A. Piedrahita *et al*., Mice lacking the folic acid-binding protein Folbp1 are defective in early embryonic development. *Nat. Genet.* **23**, 228–232 (1999).
21. L. S. Tang, R. H. Finnell, Neural and orofacial defects in Folp1 knockout mice [corrected]. *Birth Defects Res. A Clin. Mol. Teratol.***67**, 209–218 (2003). Erratum in: *Birth Defects Res. A Clin. Mol. Teratol.* 67, 473 (2003).
22. E. C. Y. Chow, M. Sondervan, C. Jin, G. M. M. Groothuis, K. S. Pang, Comparative effects of doxercalciferol (1α-hydroxyvitamin D2) versus calcitriol (1α,25-dihydroxyvitamin D3) on the expression of transporters and enzymes in the rat in vivo. *J. Pharm. Sci.* **100**, 1594–1604 (2011).
23. C. M. Pfeiffer, Z. Fazili, L. McCoy, M. Zhang, E. W. Gunter, Determination of folate vitamers in human serum by stable-isotope-dilution tandem mass spectrometry and comparison with radioassay and microbiologic assay. *Clin. Chem.* **50**, 423–432 (2004).
24. T. H. Hyun, T. Tamura, Trienzyme extraction in combination with microbiologic assay in food folate analysis: An updated review. *Exp. Biol. Med. (Maywood)* **230**, 444–454 (2005).
25. S. Aufreiter *et al*., Folate is absorbed across the colon of adults: Evidence from cecal infusion of (13)C-labeled [6S]-5-formyltetrahydrofolic acid. *Am. J. Clin. Nutr.* **90**, 116–123 (2009).
26. Y. Zhang, M. Huo, J. Zhou, S. Xie, PKSolver: An add-in program for pharmacokinetic and pharmacodynamic data analysis in Microsoft Excel. *Comput. Methods Programs Biomed.* **99**, 306–314 (2010).
27. E. C. Y. Chow, M. R. Durk, C. L. Cummins, K. S. Pang, 1Alpha,25-dihydroxyvitamin D3 up-regulates P-glycoprotein via the vitamin D receptor and not farnesoid X receptor in both fxr(-/-) and fxr(+/+) mice and increased renal and brain efflux of digoxin in mice in vivo. *J. Pharmacol. Exp. Ther.* **337**, 846–859 (2011).
28. M. R. Durk *et al*., 1α,25-Dihydroxyvitamin D3-liganded vitamin D receptor increases expression and transport activity of P-glycoprotein in isolated rat brain capillaries and human and rat brain microvessel endothelial cells. *J. Neurochem.* **123**, 944–953 (2012).
29. A. Lakoff *et al*., Folate is absorbed across the human colon: Evidence by using enteric-coated caplets containing 13C-labeled [6S]-5-formyltetrahydrofolate. *Am. J. Clin. Nutr.* **100**, 1278–1286 (2014).
30. H. J. Blom, G. M. Shaw, M. den Heijer, R. H. Finnell, Neural tube defects and folate: Case far from closed. *Nat. Rev. Neurosci.* **7**, 724–731 (2006).
31. R. E. Frye, J. M. Sequeira, E. V. Quadros, S. J. James, D. A. Rossignol, Cerebral folate receptor autoantibodies in autism spectrum disorder. *Mol. Psychiatry* **18**, 369–381 (2013).
32. A. Torres *et al*., CSF 5-methyltetrahydrofolate serial monitoring to guide treatment of congenital folate malabsorption due to proton-coupled folate transporter (PCFT) deficiency. *JIMD Rep.* **24**, 91–96 (2015).
33. D. Kronn, I. D. Goldman, *Hereditary Folate Malabsorption*, M. P. Adam *et al*., Eds. (University of Washington, Seattle, WA, 2017).
34. M. K. Lehtinen, C. A. Walsh, Neurogenesis at the brain-cerebrospinal fluid interface. *Annu. Rev. Cell Dev. Biol.* **27**, 653–679 (2011).
35. M. K. Lehtinen *et al*., The cerebrospinal fluid provides a proliferative niche for neural progenitor cells. *Neuron* **69**, 893–905 (2011).
36. X. Wang, R. M. Cabrera, Y. Li, D. S. Miller, R. H. Finnell, Functional regulation of P-glycoprotein at the blood-brain barrier in proton-coupled folate transporter (PCFT) mutant mice. *FASEB J.* **27**, 1167–1175 (2013).
37. E. C. Chow, H. Sun, A. A. Khan, G. M. Groothuis, K. S. Pang, Effects of 1α,25-dihydroxyvitamin D3 on transporters and enzymes of the rat intestine and kidney in vivo. *Biopharm. Drug Dispos.* **31**, 91–108 (2010).
38. Y. G. Assaraf, The role of multidrug resistance efflux transporters in antifolate resistance and folate homeostasis. *Drug Resist. Updat.* **9**, 227–246 (2006).
39. E. C. Y. Chow, H. P. Quach, R. Vieth, K. S. Pang, Temporal changes in tissue 1α,25-dihydroxyvitamin D3, vitamin D receptor target genes, and calcium and PTH levels after 1,25(OH)2D3 treatment in mice. *Am. J. Physiol. Endocrinol. Metab.* **304**, E977–E989 (2013).
40. P. H. Anderson, P. D. O'Loughlin, B. K. May, H. A. Morris, Quantification of mRNA for the vitamin D metabolizing enzymes CYP27B1 and CYP24 and vitamin D receptor in kidney using real-time reverse transcriptase- polymerase chain reaction. *J. Mol. Endocrinol.* **31**, 123–132 (2003).
41. H. Birn, O. Spiegelstein, E. I. Christensen, R. H. Finnell, Renal tubular reabsorption of folate mediated by folate binding protein 1. *J. Am. Soc. Nephrol.* **16**, 608–615 (2005).
42. V. T. Ramaekers, N. Blau, J. M. Sequeira, M. C. Nassogne, E. V. Quadros, Folate receptor autoimmunity and cerebral folate deficiency in low-functioning autism with neurological deficits. *Neuropediatrics* **38**, 276–281 (2007).
43. V. T. Ramaekers, E. V. Quadros, J. M. Sequeira, Role of folate receptor autoantibodies in infantile autism. *Mol. Psychiatry* **18**, 270–271 (2013).
44. R. E. Frye *et al*., Folinic acid improves verbal communication in children with autism and language impairment: A randomized double-blind placebo-controlled trial. *Mol. Psychiatry* **23**, 247–256 (2018).
45. J. Geller, D. Kronn, S. Jayabose, C. Sandoval, Hereditary folate malabsorption: Family report and review of the literature. *Medicine (Baltimore)* **81**, 51–68 (2002).
46. S. Aluri *et al*., Hereditary folate malabsorption due to a mutation in the external gate of the proton-coupled folate transporter SLC46A1. *Blood Adv.* **2**, 61–68 (2018).